(Preprint) AAS 16-316

SPIRAL LAMBERT'S PROBLEM WITH GENERALIZED LOGARITHMIC SPIRALS

Javier Roa*and Jesús Peláez†

Lambert's problem subject to a continuous acceleration is solved using the family of generalized logarithmic spirals. Thanks to the existence of two first integrals related to the energy and angular momentum surprising analogies with the Keplerian case are found. A minimum-energy spiral transfer exists. Increasing the value of the constant of the generalized energy yields pairs of conjugate spiral trajectories. The properties of such spirals are strongly connected with the properties of conjugate Keplerian orbits. When the generalized constant of the energy reaches a critical value the two solutions degenerate into a pair of parabolic spirals, one of which connects the two vectors through infinity. From that point the spiral transfers become hyperbolic. Generalized logarithmic spirals admit closed-form solutions to all the required magnitudes including the time of flight, providing a deep insight into the dynamics of the problem. In addition, the maximum acceleration along the transfer is found analytically so the solutions that violate the design constraints on the maximum thrust acceleration can be rejected without any further computations. When the time of flight is fixed there is still a degree of freedom in the solution, related to a control parameter. Resonant transfers appear naturally thanks to the symmetry properties of the generalized logarithmic spirals. The problem of designing a low-thrust transfer between two bodies can be reduced to solving the corresponding spiral Lambert's problem. In order to show the versatility of the method it is applied to the design of an asteroid tour and to explore launch opportunities to Mars.

INTRODUCTION

The problem of finding the orbit that connects two points in a given time of flight has occupied many authors throughout the years. Originally formulated by Leonard Euler and Johann H. Lambert in the 18th century, the latter's pioneering contributions motivated the problem to be called Lambert's problem. Even Gauss, the *Prince of Mathematicians*, said that this particular problem is "to be considered among the most important in the theory of the motions of the heavenly bodies". It is the core of navigation algorithms, mission design tools, and orbit determination methods. Battin's[1] improved version of Gauss' solution was implemented in the onboard guidance computer of the NASA Space Shuttle. He was totally captivated by the beauty of the problem and explored different approaches.[2] He even devoted two chapters of his book[3] to analyzing the problem, with an emphasis on collecting relevant properties. The method from Lancaster and Blanchard, originally presented in a short note,[4] was further improved by Gooding,[5] who focused on the computational aspects. He

*PhD Candidate, Space Dynamics Group, Technical University of Madrid, Pza. Cardenal Cisneros 3, 28040, Madrid. Student Member AIAA. javier.roa@upm.es

Present address: Jet Propulsion Laboratory, California Institute of Technology, 4800 Oak Grove Drive, Pasadena, CA 91109-8099, USA

†Professor and Head, Space Dynamics Group, Technical University of Madrid, Pza. Cardenal Cisneros 3, 28040, Madrid. Member AIAA.

relied on Halley's cubic iteration process to solve for the universal variable and showed that only three iterations are required for convergence. Improvements in Lancaster-Blanchard's method have also been proposed by Izzo[6]

The rise of interplanetary exploration has brought renewed interest into Lambert's problem for mission design applications, as well as into low-thrust trajectories. The combination of the two is a promising technique for mission analysts. Izzo[7] solved the spiral Lambert's problem using the exponential sinusoid, a curve proposed by Petropoulos and Longuski[8] when deriving a shape-based method for preliminary design. Unfortunately, not having an explicit expression for the time of flight forces the user to rely on numerical methods and obscures the structure of the solution.

Roa and Peláez[9,10] found a new family of solutions to the low-thrust problem, called the *generalized logarithmic spirals*. They admit closed-form expressions for all the required variables, including the time of flight. The existence of two integrals of motion yields a natural classification of the spirals in elliptic, parabolic and hyperbolic, that are closely related to Keplerian orbits. In this paper we solve Lambert's problem with the family of generalized logarithmic spirals. Thanks to the structure of the solution surprising connections with the purely ballistic case are found. Following Battin's approach, who "...collected (almost as a hobby) a number of delightful and often useful properties of the two-body, two-point boundary value problem", we pay special attention to formally stating the properties of the solution. There is a minimum energy spiral, and pairs of conjugate spirals bifurcate from it. From a practical point of view a spiral Lambert solver yields a fast and simple method for exploring preliminary solutions for low-thrust missions. Recently, the authors extended the method by introducing a control parameter[11] and considering the out-of-plane motion.[12]

The Paper is organized as follows. The next section introduces the generalized logarithmic spirals and some useful equations. Then the two-point boundary-value with free time is solved. The minimum energy spiral, the conjugate pairs and the different families of solutions are analyzed in detail in this section. The following section addresses Lambert's problem itself, fixing the time of flight. Finally, an example of application is presented.

GENERALIZED LOGARITHMIC SPIRALS

The perturbed two-body problem is governed by the differential equation

$$\frac{\mathrm{d}^2\mathbf{r}}{\mathrm{d}t^2} + \frac{\mu}{r^3}\,\mathbf{r} = \mathbf{a}_\mathrm{p}, \qquad r = \|\mathbf{r}\| \tag{1}$$

where $\mathbf{r} \in \mathbb{R}^3$ is the radiusvector of the particle, μ is the gravitational parameter of the attracting body, and $\mathbf{a}_\mathrm{p}$ denotes the perturbing acceleration. Let ψ be the flight-direction angle (complementary of the flight-path angle) and let the tangent vector be $\mathbf{t} = \mathbf{v}/v$, with $\mathbf{v}$ the velocity of the particle. Roa *et al.*[10,11] proved that for a thrust profile of the form

$$\mathbf{a}_\mathrm{p} = \frac{\mu}{r^2}[\xi\cos\psi\,\mathbf{t} + (1-2\xi)\sin\psi\,\mathbf{n}] \tag{2}$$

the system defined in Eq. (1) admits two integrals of motion. Here ξ behaves as a (constant) control parameter. In what remains of the paper the problem is normalized so that $\mu = 1$. The first integral of motion relates to the equation of the energy,

$$v^2 - \frac{2}{r}(1-\xi) = K_1, \qquad \text{with} \quad K_1 = v_0^2 - \frac{2}{r_0}(1-\xi) \tag{3}$$

where K_1 is a constant of motion defined by the initial conditions and the control parameter. The second integral of motion is a generalization of the equation of the angular momentum,

$$v^2 r \sin\psi = v r^2 \dot{\theta} = K_2 \tag{4}$$

not affected by the values of the control parameter. The constant K_2 is given by

$$K_2 = v_0^2 r_0 \sin\psi_0 \tag{5}$$

Combining Eqs. (3) and (4) provides a simple expression for the evolution of the flight-direction angle:

$$\sin\psi = \frac{K_2}{2(1-\xi) + K_1 r} \tag{6}$$

Depending on the sign of the constant of the energy K_1 three families of solutions are obtained: elliptic ($K_1 < 0$), parabolic ($K_1 = 0$) and hyperbolic ($K_1 > 0$). Elliptic spirals are bounded by a maximum radius and never escape to infinity. Parabolic spirals are logarithmic spirals. There are two types of hyperbolic spirals: spirals of Type I ($K_2 < 2(1-\xi)$) only have one asymptote, whereas spirals of Type II ($K_2 > 2(1-\xi)$) have two asymptotes. The transition between all the families is continuous.[9] Changing the value of ξ may yield transitions between spiral types.

Let $\mathcal{S}$ denote the set of generalized logarithmic spirals. Each member is defined by means of five parameters: the constant of the generalized energy, K_1, the constant of the generalized angular momentum K_2, two additional constants K_3 (fixing the orientation in the inertial reference) and K_4 (connecting the initial conditions with the time of flight), and the control parameter.

Symmetries

There are two relevant definitions regarding the symmetries found in the solution. The trajectory $r = r(\theta)$ is said to be $\mathscr{T}$-symmetric if $r(\delta + \theta_\mathrm{m}) = r(\delta - \theta_\mathrm{m})$. Here θ_m is the axis of $\mathscr{T}$-symmetry. Only elliptic spirals and hyperbolic spirals of Type II are $\mathscr{T}$-symmetric.

Equation (5) shows that two different values of ψ_0 yield the same value of K_2, provided that $\sin\psi_0$ is symmetric with respect to $\psi_0 = \pi/2$. The first possible value of ψ_0 is $\psi_0 \leq \pi/2$, whereas the second is $\psi_0 \geq \pi/2$. This means that it is possible to find two trajectories with the same values of K_1 and K_2, but differing in the regime: the first spiral is in raising regime ($\dot{r} > 0$) and the second is in lowering regime ($\dot{r} < 0$). These spirals are said to be $\mathscr{C}$-symmetric. The $\mathscr{C}$-symmetric of $\mathcal{S}$ is denoted $\mathcal{S}^\dagger$. Both spirals relate through a reflection $\mathscr{R}$ about the direction of the departure polar angle θ_0.

Elliptic spirals

Elliptic spirals are defined by $K_1 < 0$ and $K_2 \in (0, 2(1-\xi))$. They are bounded by a maximum radius

$$r_\mathrm{max} = \frac{2(1-\xi) - K_2}{(-K_1)} \tag{7}$$

so this family of spirals never escape to infinity. When the spiral reaches the maximum radius it transitions naturally from raising regime to lowering regime, and falls towards the origin. The velocity for $r = r_\mathrm{max}$ is the minimum velocity that the particle can reach,

$$v(r_\mathrm{max}) = v_\mathrm{m} = \sqrt{\frac{K_2}{r_\mathrm{max}}} = \sqrt{\frac{-K_1 K_2}{2(1-\xi) - K_2}} \tag{8}$$

The equation of the trajectory is

$$\frac{r(\theta)}{r_{\max}} = \frac{2(1-\xi)+K_2}{2(1-\xi)+K_2\cosh\beta(\theta)} \tag{9}$$

The spiral anomaly $\beta(\theta)$ can take two different values depending on the initial regime of the spiral, leading to a pair of $\mathscr{C}$-symmetric spirals:

$$\beta(\theta) = \frac{\ell}{K_2}(\theta-\theta_{\mathrm{m}}) \qquad \text{or} \qquad \beta^{\dagger}(\theta) = \frac{\ell}{K_2}(\theta-\theta_{\mathrm{m}}^{\dagger})$$

where $\ell = \sqrt{4(1-\xi)^2-K_2^2}$. Here † denotes variables corresponding to a spiral that is initially in lowering regime. The orientation of $\theta_{\mathrm{m}} = \theta(r_{\max})$ defines the axis of $\mathscr{T}$-symmetry, that is equivalent to the apse line. The axis of $\mathscr{T}$-symmetry is given by

$$\theta_{\mathrm{m}}-\theta_0 = \mp\frac{K_2}{\ell}\left|\operatorname{arccosh}\left\{\frac{r_{\max}}{r}-\frac{2(1-\xi)}{K_2}\left(1-\frac{r_{\max}}{r}\right)\right\}\right| \tag{10}$$

The first sign yields a spiral initially in raising regime ($\dot{r}_0 > 0$ and $\psi_0 < \pi/2$), whereas the second corresponds to a spiral initially in lowering regime (and it is denoted $\theta_{\mathrm{m}}^{\dagger}-\theta_0$). These solutions define different trajectories, that are $\mathscr{C}$-symmetric. In sum, the equation of the trajectory can be written $r = r(\theta;\xi,K_1,K_2,r_0,\theta_0)$.

The time of flight is given explicitly by the expression

$$t(r)-t_{\mathrm{m}} = \pm\frac{rv}{K_1}\sqrt{\frac{1-\sin\psi}{1+\sin\psi}} \pm \frac{2[2(1-\xi)k'^2\Delta\Pi-K_2\Delta\mathrm{E}]\sqrt{1-\xi}}{(-K_1)^{3/2}\sqrt{K_2}} \tag{11}$$

where $\Delta\mathrm{E}$ and $\Delta\Pi$ are the difference between the incomplete and the complete elliptic integrals of the second and third kinds, respectively, $\Delta\mathrm{E} = \mathrm{E}(\phi,k)-\mathrm{E}(k)$ and $\Delta\Pi = \Pi(\alpha;\phi,k)-\Pi(\alpha;k)$. The arguments of the elliptic integrals are

$$\sin\phi = \frac{v_{\mathrm{m}}}{v}\sqrt{\frac{2}{1+\sin\psi}}, \qquad k = \sqrt{\frac{-K_1 r_{\max}}{4(1-\xi)}}, \qquad \alpha = \frac{K_1 r_{\max}}{2K_2}, \qquad k^2+k'^2 = 1$$

The time of apoapsis passage t_{m} is solved from the initial conditions.

Parabolic spirals

Parabolic spirals ($K_1 = 0$) are equivalent to logarithmic spirals, and $K_2 \in (0, 2(1-\xi)]$. The limit case $K_2 = 0$ is a rectilinear orbit and $K_2 = 2(1-\xi)$ corresponds to degenerate parabolic spirals. Equation (6) shows that $K_2 = 2(1-\xi) \Rightarrow \psi = \pi/2$. Since the flight-path angle is constant it will remain equal to $\pi/2$. This cancels the thrust defined in Eq. (2), so the resulting trajectory is a circular Keplerian orbit. The velocity in the spiral takes the form $v = \sqrt{2(1-\xi)/r}$, and does not necessarily coincide with the circular velocity.

Given the expression for the velocity it follows that parabolic spirals reach infinity with zero velocity, just like parabolic Keplerian orbits. The flight-direction angle remains constant and the trajectory is not bounded. If the spiral is initially in lowering regime it will always fall towards the

origin, and if it departs from raising regime it will always escape to infinity. The equation of the trajectory is simply

$$r(\theta) = r_0\, \mathrm{e}^{(\theta-\theta_0)\cot\psi} \tag{12}$$

The time of flight when $K_1 = 0$ reduces to

$$t(r) - t_0 = \pm\frac{2\sqrt{2(1-\xi)}}{3\ell}\left(r^{3/2} - r_0^{3/2}\right) \tag{13}$$

where $\ell = \sqrt{4(1-\xi)^2 - K_2^2} = \cos\psi$. The particle requires an infinite time to reach infinity.

Hyperbolic spirals

Hyperbolic spirals are defined by a positive constant of the energy, $K_1 > 0$, in analogy with the definition given to hyperbolic Keplerian orbits. They reach infinity with a finite, nonzero velocity $v_\infty^2 = K_1$. Two different subfamilies can be distinguished depending of the value of K_2: *i)* Type I: hyperbolic spirals with $K_2 < 2(1-\xi)$. They only have one asymptote. *ii)* Type II: hyperbolic spirals with $K_2 > 2(1-\xi)$. They have two asymptotes and they are $\mathscr{T}$-symmetric. Type I and Type II spirals are separated by the limit case $K_2 = 2(1-\xi)$, and the transition is continuous.[10]

Type I hyperbolic spirals The dynamics of Type I hyperbolic spirals is simple, since there are no natural transitions between regimes. Like in the case of parabolic spirals if the spiral is in lowering regime it falls towards the origin, and it escapes to infinity if in raising regime.

The equation of the trajectory takes the form

$$r(\theta) = \frac{\zeta\ell^2/K_1}{\sinh\frac{\beta}{2}\left[4\zeta(1-\xi)\sinh\frac{\beta}{2} + (\zeta^2 - K_2^2)\cosh\frac{\beta}{2}\right]} \tag{14}$$

with $\zeta = 2(1-\xi) - \ell$ and

$$\beta = \frac{\ell}{K_2}(\theta_{\mathrm{as}} - \theta), \qquad \beta^\dagger = -\frac{\ell}{K_2}(\theta_{\mathrm{as}}^\dagger - \theta)$$

The direction of the asymptote is θ_{as}:

$$\theta_{\mathrm{as}} - \theta_0 = \pm\frac{K_2}{\ell}\ln\left[\frac{K_2(\zeta - \ell - K_2\sin\psi_0 + \ell\,|\cos\psi_0|)}{r_0 K_1 \zeta\sin\psi_0}\right]$$

These expressions relate Eq. (14) with the initial conditions (r_0, θ_0). The time of flight to a given radius reads

$$t(r) = K_4 \pm \left\{\frac{rv}{K_1}\sqrt{\frac{1+\sin\psi}{1-\sin\psi}} - \frac{2\left[\mathrm{E} - (1-\alpha)\Pi\right]\sqrt{K_2(1-\xi)}}{K_1^{3/2}}\right\} \tag{15}$$

with

$$\sin\phi = \sqrt{\frac{K_1 r\sin\psi}{\alpha K_2(1-\sin\psi)}}, \qquad k = \frac{1}{2}\sqrt{\frac{2(1-\xi)+K_2}{1-\xi}}, \qquad \alpha = \frac{2(1-\xi)+K_2}{2K_2}$$

The constant K_4 is solved from the initial conditions.

Type II hyperbolic spirals Hyperbolic spirals with $K_2 > 1$ are bounded by a minimum radius

$$r_{\min} = \frac{K_2 - 2(1-\xi)}{K_1} \tag{16}$$

so that the spirals can never reach the origin. If the spiral is initially in lowering regime it reaches the minimum radius, transitions to raising regime and then escapes. The velocity at $r_{\min}$ is maximum,

$$v(r_{\min}) = v_{\mathrm{m}} = \sqrt{\frac{K_1 K_2}{K_2 - 2(1-\xi)}} \tag{17}$$

The trajectory is defined by the equation:

$$\frac{r(\theta)}{r_{\min}} = \frac{2(1-\xi) + K_2}{2(1-\xi) + K_2 \cos\beta} \tag{18}$$

with the spiral anomaly defined as

$$\beta = \frac{\ell}{K_2}(\theta - \theta_{\mathrm{m}}) \qquad \text{or} \qquad \beta^{\dagger} = \frac{\ell}{K_2}(\theta - \theta_{\mathrm{m}}^{\dagger})$$

depending on the initial regime of the spiral. In this case it is $\ell = \sqrt{K_2^2 - 4(1-\xi)^2}$. The previous equation is $\mathscr{T}$-symmetric with respect to $\theta_{\mathrm{m}} = \theta(r_{\min})$, which is aligned with the periapsis of the spiral. The orientation of $r_{\min}$ is given by

$$\theta_{\mathrm{m}} - \theta_0 = \mp \frac{K_2}{\ell}\left\{\frac{\pi}{2} + \arctan\left[\frac{2(1-\xi) - K_2 \sin\psi_0}{\ell\,|\cos\psi_0|}\right]\right\} \tag{19}$$

The sign in this expression depends on the regime of the spiral.

The time of flight is referred to the time to periapsis passage t_{m} by means of

$$\begin{aligned} t(r) - t_{\mathrm{m}} = \mp\Bigg\{ & \frac{[K_2 + 2(1-\xi)]K_2 \mathrm{E} - K_1 r_{\min}[K_2 \mathrm{F} + 2(1-\xi)\Pi]}{K_1\sqrt{K_1 K_2 [K_2 + 2(1-\xi)]}} \\ & + \frac{2(1-\xi)}{K_1^{3/2}} \operatorname{arcsinh}\left[\frac{\sqrt{2K_1 r(rv^2 - K_2)}}{2\sqrt{K_2 r v^2 + (rv^2 - K_2)(1-\xi)}}\right] - \frac{v}{K_1^2}\sqrt{r^2 v^4 - K_2^2}\Bigg\} \end{aligned} \tag{20}$$

with $z = 1 + K_1 r$. In this case the arguments of the elliptic integrals are

$$\sin\phi = \frac{\sqrt{2(1-\xi)(1-\sin\psi)}}{k\sqrt{K_2 - 2(1-\xi)\sin\psi}}, \quad k = \frac{2\sqrt{1-\xi}}{\sqrt{K_2 + 2(1-\xi)}}, \quad n = \frac{2(1-\xi)}{K_2}$$

The time of flight to the periapsis, t_{m}, is solved from Eq. (20) particularized at $r = r_0$.

Osculating elements

The orbital elements defining the osculating orbit can be referred to the constants defining the spirals and the radial distance. In particular, the eccentricity reads

$$e(r) = \sqrt{K_2^2 + 1 - 2K_2 \sin\psi} \tag{21}$$

The angular momentum relates to the constant K_2: Roa *et al.*[10] connect Eq. (4) with the torque from the perturbed forces, and from that derivation it follows

$$h(r) = K_2 \sqrt{\frac{r}{2(1-\xi) + K_1 r}} \tag{22}$$

The semimajor axis is obtained by combining Eqs. (21) and (22), and results in

$$a(r) = \frac{h^2}{1-e^2} = \frac{r}{2\xi - K_1 r} \tag{23}$$

The semimajor axis always grows in raising regime and decreases in lowering regime, no matter the type of spiral.

THE TWO-POINT BOUNDARY-VALUE PROBLEM

Consider the problem of finding a generalized logarithmic spiral $\mathcal{S}$ that connects a departure point $\mathcal{P}_1$, defined by (r_1, θ_1), with a final point $\mathcal{P}_2$, defined by (r_2, θ_2), with $\theta_2 > \theta_1$, and given the value of the control parameter. The position vectors for $\mathcal{P}_1$ and $\mathcal{P}_2$ are $\mathbf{r}_1$ and $\mathbf{r}_2$, respectively. In order to account for the number of revolutions n, θ_2 is decomposed in $\theta_2 = \tilde{\theta}_2 + 2n\pi$, with $n = 0, 1, 2 \ldots$ and $\tilde{\theta}_2 \in [0, 2\pi]$. Changing the number of revolutions is equivalent to modifying the geometry of the boundary value problem (BVP). No constraints are imposed on the time of flight in this section. In order the trajectory to depart from $\mathcal{P}_1$ and arrive to $\mathcal{P}_2$ the following equation must be satisfied:

$$r_2 = r(\theta_2; \xi, K_1, K_2, r_1, \theta_1) \tag{24}$$

The function $r(\theta; \xi, K_1, K_2, r_1, \theta_1)$ is the equation of the trajectory and depends on the type of spiral; the polar angle θ is the independent variable, the constants K_1 and K_2 define the shape of the spiral, (r_1, θ_1) are the initial conditions at $\mathcal{P}_1$, and ξ is the control parameter. Table 1 summarizes the equations of the trajectory for the different families of solutions.

Table 1: **Summary of equations for the different families of generalized logarithmic spirals**

Type of spiral	K_1	K_2	Trajectory	Time of flight
Elliptic	< 0	$(0, 2(1-\xi))$	(9)	(11)
Parabolic	$= 0$	$(0, 2(1-\xi)]$	(12)	(13)
Hyperb. T-I	> 0	$(0, 2(1-\xi))$	(14)	(15)
Hyperb. T-II	> 0	> 1	(18)	(20)

Note: The limit case $K_2 = 1$ is omitted for brevity. It is formulated in the original paper.[9]

In the Keplerian case the minimum energy ellipse plays a key role in the configuration of the transfers.[3] The Keplerian energy (or equivalently the semimajor axis of the orbit) yields an intuitive parameterization of the solutions. An analogous parameterization can be introduced for the spiral case in terms of the constant K_1. With this technique the solutions are easily classified in elliptic, parabolic or hyperbolic spiral transfers.

Given the boundary conditions (r_1, θ_1) and (r_2, θ_2) there are *two degrees of freedom*. When fixing K_1 and ξ the problem reduces to solving for K_2 in Eq. (24). The departure velocity reads:

$$v_1 = \sqrt{K_1 + \frac{2(1-\xi)}{r_1}} \quad \text{and} \quad v_2 = \sqrt{K_1 + \frac{2(1-\xi)}{r_2}}$$

If the initial and final radii are the same, $r_1 = r_2$, the departure and terminal velocities in a generalized spiral trajectory are also equal, $v_1 = v_2$.

From the definition of the semimajor axis Roa *et al.*[10] found a practical property:

Property 1: *(Change in the semimajor axis) Given ξ, the change in the inverse of the semimajor axis between two points of the spiral depends on r_1 and r_2 alone, and reduces to:*

$$\frac{1}{a_2} - \frac{1}{a_1} = 2\xi\left(\frac{1}{r_2} - \frac{1}{r_1}\right)$$

Since K_1, ξ and r_1 are fixed Eq. (6) shows that solving for K_2 is equivalent to solving for the initial flight-direction angle, ψ_1. In fact, due to the $\mathscr{C}$-symmetry of the spirals it is more convenient to solve for the departure angle ψ_1 in order not to lose any solution, and then compute the value of K_2 from Eq. (6).

Elliptic spirals are those with the minimum value of the constant of the energy K_1, as shown in Table 1. In this case the BVP reduces to finding the zeros of the function

$$f(\psi_1) \equiv \frac{r_2}{r_{\max}} - \frac{2(1-\xi) + K_2}{2(1-\xi) + K_2 \cosh\beta_2} = 0 \qquad (25)$$

where β_2 is the spiral anomaly at $\mathcal{P}_2$.

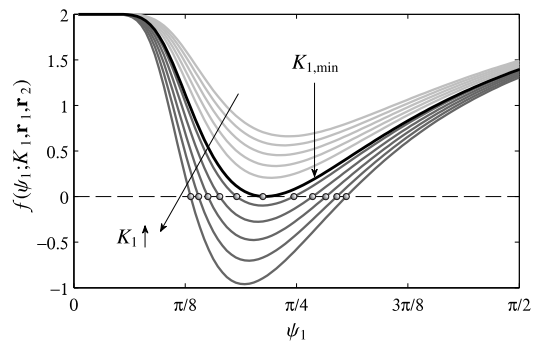

Figure 1: **Zeros of the function $f(\psi_1)$ for increasing values of $K_1 < 0$**

Figure 1 shows the effect of the constant K_1 on the zeros of the function $f(\psi_1)$ for an example transfer geometry. This figure proves that a minimum value of K_1 exists: for $K_1 > K_{1,\min}$ there are two solutions, that collapse to one double solution when $K_1 = K_{1,\min}$. If $K_1 < K_{1,\min}$ the function has no roots: the BVP has no solution. Similarly, there is a maximum value of ξ, $\xi_{\max}$, above which the problem has no solution.

The minimum-energy spiral

Let $\mathbb{S}$ denote the set of all generalized logarithmic spirals $\mathcal{S}$ that are solutions to the BVP. The elliptic spiral for which $K_1 = K_{1,\min}$ is referred to as the *minimum-energy spiral*, $\mathcal{S}_{\mathrm{m}} \in \mathbb{S}$. The constant of the energy relates to the specific Keplerian energy E_{k} by means of

$$K_1 = 2\left(E_{\mathrm{k}} + \frac{\xi}{r}\right)$$

Consider two spirals $\mathcal{S}_i, \mathcal{S}_j \in \mathbb{S}$, with $i \neq j$. The corresponding values of K_1 can be solved from the previous particularized at r_1 and $E_{k,i}$ or $E_{k,j}$, respectively. If ξ is given and $\mathcal{S}_i$ is the minimum-energy spiral ($i \equiv \mathrm{m}$), then the osculating Keplerian energy at r_1 is also minimum:

Property 2: *(Minimum Keplerian energy) The osculating orbits at $\mathcal{P}_1$ and $\mathcal{P}_2$ for the minimum energy spiral are those with the minimum Keplerian energy and semimajor axis.*

In addition, from the definition of the velocity it follows

Property 3: *(Minimum velocity) The departure and terminal velocities, v_1 and v_2, are minimum on the minimum-energy spiral.*

The minimum energy spiral satisfies the following property regarding the change in the velocity and semimajor axis in the transfer from $\mathcal{P}_1$ to $\mathcal{P}_2$:

Property 4: *(Change in the velocity and semimajor axis) The change in the velocity from $\mathcal{P}_1$ to $\mathcal{P}_2$, $\Delta v = |v_2 - v_1|$, is maximum along the minimum-energy spiral. Similarly, the change in the semimajor axis, $|\Delta a| = |a_2 - a_1|$, is minimum along the minimum-energy spiral.*

The value of $K_{1,\min}$ can be obtained through the following numerical procedure. The function $f(\psi_1)$ defined in Eq. (25) reaches a minimum at ψ_1^*, so that $f'(\psi_1^*; K_1, \xi, \mathbf{r}_1, \mathbf{r}_2) = 0$. The prime $()'$ denotes the derivative with respect to ψ_1. The minimum value of K_1 for which a solution to the boundary value problem exists corresponds to the value that yields only one root of the function $f(\psi_1)$. That is, when the minimum of $f(\psi_1)$ is exactly zero. Given the boundary conditions $\mathbf{r}_1$ and $\mathbf{r}_2$, and the value of ξ, the minimum-energy transfer, defined by $K_{1,\min}$ and ψ_1^*, is the spiral that satisfies

$$f\ (\psi_1^*; K_{1,\min}, \xi, \mathbf{r}_1, \mathbf{r}_2) = 0 \tag{26}$$

$$f'(\psi_1^*; K_{1,\min}, \xi, \mathbf{r}_1, \mathbf{r}_2) = 0 \tag{27}$$

The first condition forces the minimum to be zero, so there is only one root, and the second equation determines where the minimum is located. Note that $K_{1,\min}$ is defined in terms of $\theta_2 = \tilde{\theta}_2 + 2n\pi$ and takes different values depending on the number of revolutions n, even if $\tilde{\theta}_2$ remains the same.

Figure 2 shows how the value of $K_{1,\min}$ depends on the geometry of the transfer. As the transfer angle increases the value of $K_{1,\min}$ decreases in magnitude, meaning that increasing the number of revolutions reduces the energy of the transfer. The evolution of the values of $K_{1,\min}$ proves that $\lim_{\theta_2 \to \infty} K_{1,\min} = 0^-$; transfers with negative K_1 always exist, and the magnitude of the constant K_2 can be arbitrarily small. This yields an important result, which is that the BVP defined by $\mathbf{r}_1$ and $\mathbf{r}_2$ will always admit three types of solutions: elliptic, parabolic and hyperbolic spiral transfers.

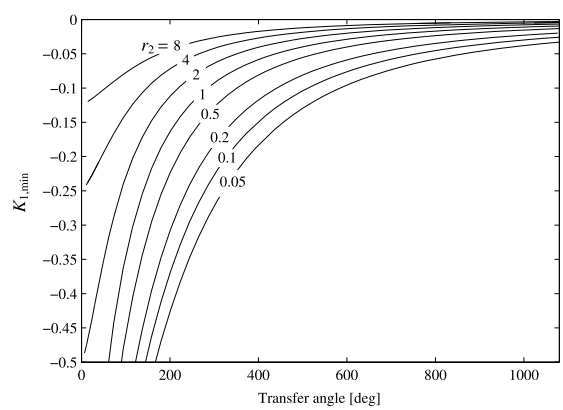

Figure 2: **Minimum K_1 for different tranfer geometries and fixed ξ**

Conjugate spirals

The existence of two solutions to Eq. (25) for each value of the constant of the energy and control parameter has already been anticipated. This behavior is intimately related to the conjugate Keplerian orbits that appear in the unperturbed form of Lambert's problem:[3]

Definition 1: *(Conjugate spirals) Two generalized logarithmic spirals $\mathcal{S}, \tilde{\mathcal{S}} \in \mathbb{S}$ are said to be conjugate if they share the same value of the constant of the energy K_1, and ξ. The conjugate of $\mathcal{S}$ is $\tilde{\mathcal{S}}$.*

Figure 3 shows the spiral transfer corresponding to $K_{1,\min}$ and two pairs of conjugate spirals, $\mathcal{S}_i$ and $\tilde{\mathcal{S}}_i$. A spiral and its conjugate are always separated by the minimum energy spiral. As K_1 becomes more negative both trajectories come closer, and they collapse into one single trajectory,

$\mathcal{S}_\mathrm{m}$, for $K_1 = K_{1,\min}$. In this example both the spiral $\mathcal{S}_i$ and its conjugate $\tilde{\mathcal{S}}_i$ reach $\mathcal{P}_2$ in lowering regime, after having crossed the maximum radius r_max.

Given a pair of conjugate solutions to the BVP, one will be faster than the minimum-energy transfer, whereas its conjugate will be slower. Conjugate spirals can be characterized by a collection of properties connecting the values that certain variables take at departure and arrival. In order to establish such properties it is important to note that:

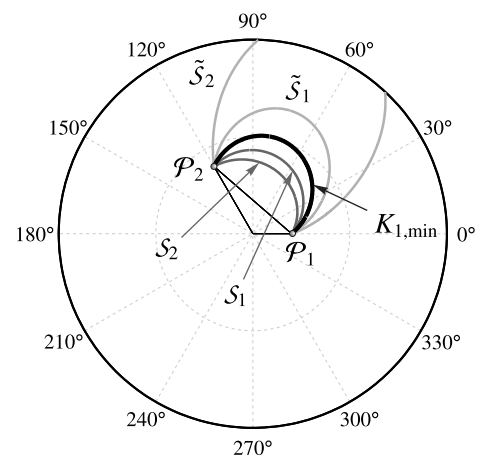

Figure 3: **Pairs of conjugate spiral transfers**

Lemma 1: *If a certain variable γ depends only on K_1, ξ and r, $\gamma = \gamma(r; K_1)$, then $\gamma_1 = \tilde{\gamma}_1$ and $\gamma_2 = \tilde{\gamma}_2$ for all pairs of conjugate spirals. Here $\gamma_1 = \gamma(r_1)$ and $\gamma_2 = \gamma(r_2)$.*

This Lemma is a powerful contrivance for finding variables that take the same values on a spiral and its conjugate (locally). Equation (3) shows that the velocity is a function of the form

$$v = \sqrt{K_1 + \frac{2(1-\xi)}{r}} = v(r; K_1, \xi)$$

and by Lemma 1 it follows

Property 5: *(Departure and terminal velocities) Two conjugate generalized logarithmic spirals $\mathcal{S}$ and $\tilde{\mathcal{S}}$ have the same departure and terminal velocity, i.e. $v_1 = \tilde{v}_1$ and $v_2 = \tilde{v}_2$.*

Property 6: *(Departure and terminal semimajor axes) Two conjugate spirals $\mathcal{S}$ and $\tilde{\mathcal{S}}$ have the same departure and terminal osculating semimajor axes, i.e. $a_1 = \tilde{a}_1$ and $a_2 = \tilde{a}_2$.*

Consider the variables that also depend on K_2 but that can be decomposed in $\gamma = g(K_2)\,\gamma^*(r; K_1, \xi)$. Here g is an arbitrary function of K_2 and γ^* does not depend on K_2. The ratio between the initial and final values of γ for the transfer along $\mathcal{S}$, γ_2/γ_1, no longer depends on K_2 and Lemma 1 is applicable. This technique yields a number of useful additional properties:

Property 7: *(Angular velocities) The ratio between the initial and terminal angular velocities is the same for two conjugate spirals, $\dot{\theta}_1/\dot{\theta}_2 = \tilde{\dot{\theta}}_1/\tilde{\dot{\theta}}_2$.*

Property 8: *(Flight-direction angle) The ratio between the initial and terminal values of $\sin\psi$ is the same for two conjugate spirals, $\sin\psi_1/\sin\psi_2 = \sin\tilde{\psi}_1/\sin\tilde{\psi}_2$.*

Property 9: *(Circumferential velocities) The ratio between the initial and terminal circumferential velocities is the same for two conjugate spirals, $v_{\theta 1}/v_{\theta 2} = \tilde{v}_{\theta 1}/\tilde{v}_{\theta 2}$.*

Property 10: *(Angular momentum) The ratio between the initial and terminal angular momenta (or equivalently the orbital parameter, p) is the same for two conjugate spirals, $h_1/h_2 = \tilde{h}_1/\tilde{h}_2$ and $p_1/p_2 = \tilde{p}_1/\tilde{p}_2$.*

Property 11: *(Eccentricity) The initial and terminal values of the eccentricity of two conjugate spirals satisfy the relation* $(1 - e_1^2)/(1 - e_2^2) = (1 - \tilde{e}_1^2)/(1 - \tilde{e}_2^2)$.

Families of solutions

Parameterizing the solutions of the BVP in terms of K_1 (keeping ξ fixed) yields a natural classification of the solutions: starting from $K_{1,\min} < 0$, the spirals are elliptic in the interval $K_1 \in [K_{1,\min}, 0)$; solutions with $K_1 = 0$ are parabolic spirals, and for $K_1 > 0$ the spirals are hyperbolic.

Figure 4 shows an illustrative example of the families of solutions for a given ξ. First note that the minimum-energy spiral separates the fast and slow transfers along elliptic spirals. Reducing the value of K_1 makes the pairs of conjugate spirals to converge to the minimum-energy spiral. On the contrary, increasing K_1 reduces the size of the fast transfers and increases the size of the slow ones. The limits are set by the corresponding parabolic spirals ($K_1 = 0$). The solution to the transfer along a parabolic (logarithmic) spiral can be given in closed-form. The constraint in Eq. (24) combined with Eq. (12) provides

$$r_2 = r_1\, \mathrm{e}^{(\theta_2-\theta_1)\cot\psi_1} \implies \psi_1 = \arctan\left[\frac{\theta_2-\theta_1}{\ln(r_2/r_1)}\right] \quad (28)$$

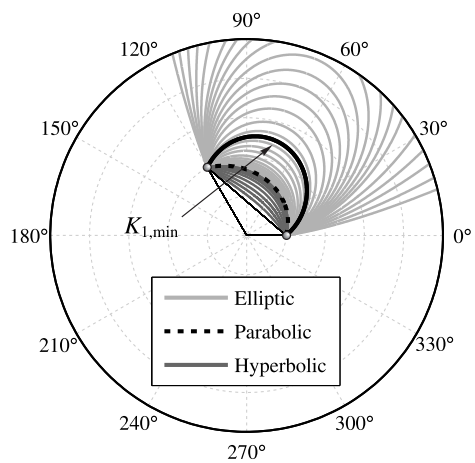

Figure 4: **Families of solutions**

and defines the departure flight-direction angle. If the spiral is in lowering regime, $r_2 < r_1$, the solution to Eq. (28) is negative and then the departure angle takes the value $\pi + \psi_1$. Equivalently the value of K_2 results in

$$K_2 = \frac{2b(1-\xi)}{\sqrt{1+b^2}} \qquad \text{with } b = \frac{\theta_2-\theta_1}{\ln(r_2/r_1)} \quad (29)$$

This value of K_2 is unique no matter the regime of the spiral, thanks to the $\mathscr{C}$-symmetry of the trajectory. It does not depend on ξ neither. Equation (28) has only one solution: the second conjugate solution is not real, since it connects both points through infinity. That is equivalent to an elliptic spiral with $r_{\max} \to \infty$. If K_1 increases it becomes positive and yields hyperbolic spirals. Pairs of conjugate solutions also exist in this case, one of them being a fictitious solution through infinity. The fast transfers are below the parabolic transfer and connect the two points directly. In the limit $K_1 \to \infty$ the hyperbolic spiral degenerates into a rectilinear orbit along the chord connecting $\mathbf{r}_1$ and $\mathbf{r}_2$. The conjugate solutions connect the two points by reaching infinity, so the

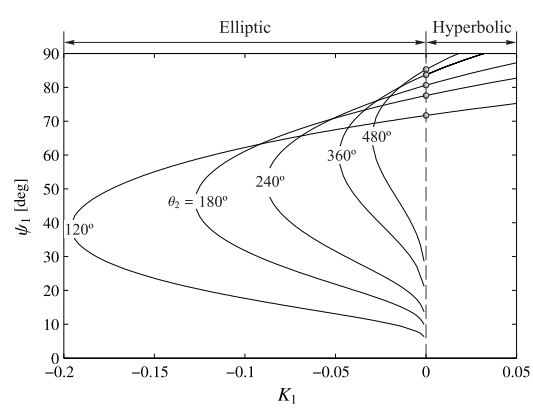

Figure 5: **Departure flight-direction angle as a function of** K_1

solution does not exist in practice. In the multi-revolution case the transfer for $K_1 \to \infty$ decomposes into two rectilinear segments connecting $\mathcal{P}_1$ with the origin and the origin with $\mathcal{P}_2$.

The existence of conjugate spirals and the discussed behavior can be understood from Fig. 5. There are two elliptic spiral transfers with the same value of K_1 and ξ. For $K_1 = K_{1,\min}$ the pair of conjugate spirals converge to the minimum energy spiral, and for $K_1 \to 0^-$ the apoapsis of the slow transfer becomes infinite. The branch of fast transfers ($\psi_1 > \psi_{1,\mathrm{m}}$) exists for both the parabolic and hyperbolic cases, but the slow transfers ($\psi_1 < \psi_{1,\mathrm{m}}$) exist only for the elliptic case. The branch of conjugate slow hyperbolic solutions corresponds to fictitious transfers through infinity, just like Keplerian hyperbolas. Despite the fact that the minimum energy spiral $\mathcal{S}_\mathrm{m}$ always departs with $\psi_1 \in (0, \pi/2)$, this constraint does not apply to generic fast transfers: arbitrary solutions with $\psi_1 \geq \pi/2$ can be found.

The trajectory of a particle following a hyperbolic spiral ($K_1 > 0$) takes different forms depending on the value of K_2, the transition being $K_2 = 2(1-\xi)$. It is possible to find a limit value of K_1, $K_{1,\mathrm{tr}}$, such that if $K_1 < K_{1,\mathrm{tr}}$ then $\mathcal{S} \in \mathbb{S}$ is hyperbolic of Type I, and of Type II for $K_1 > K_{1,\mathrm{tr}}$. It reads

$$K_{1,\mathrm{tr}} = \frac{4(1-\xi)[2\sqrt{(r_2-r_1)^2 + r_1 r_2 \Delta\theta^2} - (r_2+r_1)\Delta\theta]}{r_1 r_2 \Delta\theta(4-\Delta\theta^2)} \tag{30}$$

with $\Delta\theta = \theta_2 - \theta_1$. When $K_{1,\mathrm{tr}} \to 0$ all hyperbolic spirals in $\mathbb{S}$ are of Type II. It is interesting to note that for transfers where $r_2 = r_1$ it is $K_{1,\mathrm{tr}} = 0$, which yields the property:

Property 12: *(Hyperbolic spirals for $r_1 = r_2$) For $r_1 = r_2$ all hyperbolic spirals $\mathcal{S} \in \mathbb{S}$ are of Type II.*

For $r_1 = r_2$ the direction of the axis of $\mathcal{T}$-symmetry θ_m reduces to $\theta_\mathrm{m} = (\theta_2 + \theta_1)/2$. In his book,[3] Battin discusses a number of properties involving the bisection of the transfer angle. In the spiral case we found that:

Property 13: *(Axis of $\mathcal{T}$-symmetry and the bisection) For transfers with $r_1 = r_2$ all spiral solutions are $\mathcal{T}$-symmetric and the axis of $\mathcal{T}$-symmetry coincides with the bisection of the transfer angle.*

The dynamics of the transfer depend on whether the spiral transitions between regimes or not. For a formal treatment of the solutions we introduce the following definition:

Definition 2: *(Direct and indirect transfers) A spiral transfer $\mathcal{S} \in \mathbb{S}$ is* direct *if the evolution of the radius r from r_1 to r_2 is monotonic. On the contrary, if r reaches a minimum or maximum value during the transfer, then the solution is an* indirect *transfer. Indirect transfers can only be elliptic or hyperbolic spirals of Type II, and the axis of $\mathcal{T}$-symmetry lies between θ_1 and θ_2, $\theta_\mathrm{m} \in [\theta_1, \theta_2]$.*

To determine whether a solution $\mathcal{S} \in \mathbb{S}$ is direct or indirect one should solve for θ_m in Eqs. (10a) or (19b) and check if it lies between θ_1 and θ_2. Similarly, these relations are useful when looking explicitly for direct or indirect transfers. A direct consequence of Prop. 12 is:

Property 14: *(Indirect transfers for $r_1 = r_2$) All spiral transfers $\mathcal{S} \in \mathbb{S}$ connecting $r_1 = r_2$ are indirect. The case $K_1 = 0$ yields a degenerate indirect transfer, corresponding to a circular Keplerian orbit.*

The thrust acceleration

The thrust acceleration profile is defined in Eq. (2), and depends on the radial distance, the flight-direction angle and the control parameter. Figure 6 depicts the evolution of the acceleration due to the thrust for different types of spirals. Initially the acceleration is maximum for slow elliptic transfers. It decreases rapidly and vanishes for $r = r_{\max}$. When the spiral transitions to lowering regime the acceleration changes its sign. The figure shows how the acceleration profile resembles the typical thrust-coast-thrust sequence. The minimum energy transfer separates the slow and the fast elliptic spiral transfers. The acceleration along hyperbolic spirals of Type II is zero for $r = r_{\min}$, and also $a_{\mathrm{p}} \to 0$ as $r \to \infty$. That is, the magnitude of the thrust acceleration decreases along the asymptotes. The thrust along parabolic or Type I hyperbolic spirals never vanishes, because there are no transitions between regimes.

Negative values of the acceleration oppose the velocity. For indirect elliptic spiral transfers the acceleration will always be positive at departure, vanish when $r = r_{\max}$ and then become negative. Similarly, the acceleration along indirect hyperbolic transfers of Type II will always be negative at departure, vanish at $r = r_{\min}$ and then become positive. For direct transfers the sign of the acceleration depends on the geometry of the transfer: if $r_1 > r_2$ the acceleration will always be positive, and negative when $r_1 < r_2$. When $r_1 = r_2$ Prop. 14 proved that all spiral transfers are indirect, except for $K_1 = 0$ that yields degenerate parabolic spirals.

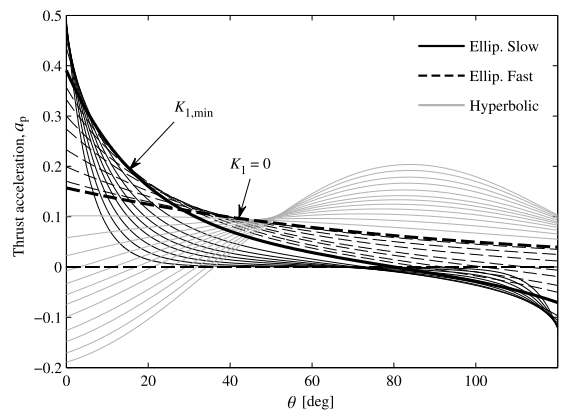

Figure 6: **Thrust acceleration (fixed ξ)**

In practice, knowing a priori the maximum value of the thrust greatly helps in the design process, since solutions that require a propulsive acceleration over the admissible maximum can be easily discarded. The magnitude of the acceleration due to the thrust $\mathbf{a}_{\mathrm{p}}$ takes the form

$$a_{\mathrm{p}}(r) = \frac{1}{r^2}\sqrt{\xi^2\cos^2\psi + (1-2\xi)^2\sin^2\psi} = \frac{\sqrt{\xi^2[2(1-\xi)+K_1 r]^2 + K_2^2(1-4\xi+3\xi^2)}}{r^2[2(1-\xi)+K_1 r]}$$

The thrust magnitude depends on K_1, K_2, ξ and the radial distance. Once the transfer spiral is selected the problem of finding the maximum value of $a_{\mathrm{p}}(r)$ reduces to finding the radius r^* that maximizes $a_{\mathrm{p}}(r)$, so that

$$a_{\mathrm{p,max}} = \frac{\sqrt{\xi^2[2(1-\xi)+K_1 r^*]^2 + K_2^2(1-4\xi+3\xi^2)}}{r^{*2}[2(1-\xi)+K_1 r^*]} \tag{31}$$

Depending on the type of spiral r^* takes different forms. In particular:

Property 15: *(Maximum thrust acceleration) The maximum acceleration exerted by the thrust* $\mathbf{a}_{\mathrm{p}}$ *along a spiral transfer from* $\mathbf{r}_1$ *to* $\mathbf{r}_2$ *occurs at* $r^* = \min(r_1, r_2)$*, except for the case of hyperbolic spirals of Type II, where* r^* *is given by Eq.* (32).

$$\xi \in [\xi^-, \xi^+] : \begin{cases} \min(r_1, r_2), & r_Q \leq \min(r_1, r_2), \text{ D} \\ \max(r_1, r_2), & r_Q \geq \max(r_1, r_2), \text{ D} \\ r_Q, & \text{rest} \end{cases} ; \qquad \xi \notin [\xi^-, \xi^+] : \begin{cases} r_{\min}, & \text{I} \\ \min(r_1, r_2), & \text{rest} \end{cases} \tag{32}$$

Here D and I denote direct and indirect transfers, respectively. The value of r_Q is:

$$r_Q = \frac{6K_1K_2(1-\xi)}{R^{1/3}} \left[(1-3\xi)K_2 \cos\left(\frac{\vartheta + 2\pi}{3}\right) - \xi\sqrt{2(1-\xi)(3\xi-1)} \right]$$

where

$$R = 54K_1^6K_2^3\xi^3\sqrt{2(3\xi-1)^3(1-\xi)^3}, \qquad \vartheta = \arctan\left[\frac{\sqrt{2[K_2^2(3\xi-1) - 2\xi^2(1-\xi)]}}{2\xi\sqrt{1-\xi}} \right]$$

The limits ξ^+ and ξ^- are the solutions to the equation

$$\frac{|1-2\xi|}{r_{\min}^2} = \frac{\sqrt{\xi^2[2(1-\xi) + K_1 r_Q]^2 + K_2^2(1-4\xi+3\xi^2)}}{{r_Q}^2[2(1-\xi) + K_1 r_Q]}$$

and determine the values of ξ that make the acceleration at the periapsis of the spiral to match the acceleration at r_Q. Property 15 helps in finding where the maximum acceleration due to the thrust occurs. The constraint on K_2 becomes:

$$K_2^2 \leq \frac{a_{\text{p,max}}^2 r^{*4}[2(1-\xi) + K_1 r^*]^2 - \xi^2[2(1-\xi) + K_1 r^*]^2}{1 - 4\xi + 3\xi^2}$$

This expression leads to a criterion for bounding the search in the space of solutions.

Total Δv

The total Δv imparted to the particle by the continuous thrust is defined by the integral

$$\Delta v_{\text{tot}} = \int_{t_1}^{t_2} a_{\text{p}}\, \mathrm{d}t = \int_{t_1}^{t_2} \frac{1}{r^2}\sqrt{\xi^2\cos^2\psi + (1-2\xi)^2\sin^2\psi}\, \mathrm{d}t \tag{33}$$

In general this equation needs to be evaluated numerically. Under the assumption that the specific impulse is constant the rocket equation will provide the mass fraction from the value of Δv_{tot}. In the special case $\xi = 1/2$ (purely tangential thrust) the previous integral can be solved in closed form. For direct transfers it is:

$$\Delta v_{\text{tot}} = \left| \sqrt{K_1 + \frac{1}{r_1}} - \sqrt{K_1 + \frac{1}{r_2}} \right| = |v_1 - v_2| \tag{34}$$

The total Δv imparted by the thrust does not depend on the path, it only depends on the initial and final velocities. From the property of the departure and terminal velocities along conjugate spirals (Prop. 5) it follows:

Property 16: *(Conjugate Δv_{tot} with tangential thrust) The total change in the velocity due to the tangential acceleration from Eq.* (2) *with $\xi = 1/2$ along two conjugate direct spirals is the same.*

Property 4 states that the difference between the departure and arrival velocities $|v_2 - v_1|$ along the minimum energy spiral $\mathcal{S}_\mathrm{m}$ is maximum. Thus, if the minimum energy spiral defines a direct transfer, then the resulting Δv_tot is the maximum among all the possible direct transfers.

If the spiral transfer is indirect it reaches a maximum or minimum radius r_m during the transfer, and the Δv_tot reads:

$$\Delta v_\mathrm{tot} = |v_1 - v_\mathrm{m}| + |v_2 - v_\mathrm{m}| = \left| \sqrt{K_1 + \frac{2(1-\xi)}{r_1}} + \sqrt{K_1 + \frac{2(1-\xi)}{r_2}} - 2\sqrt{\frac{K_1 K_2}{K_2 - 2(1-\xi)}} \right| \tag{35}$$

This expression depends on K_1 but also on K_2, by means of the velocity at the extreme point. Since two conjugate spirals are defined by different values of K_2, the total Δv_tot is different.

The locus of velocities

Figure 7 depicts the locus of velocity vectors projected on skewed axes.[3] The departure velocity vector $\mathbf{v}_1$ decomposes in

$$\mathbf{v}_1 = v_\rho\, \mathbf{u}_1 + v_\mathrm{c}\, \mathbf{u}_\mathrm{c}$$

where $\mathbf{u}_1 = \mathbf{r}_1/r_1$ and $\mathbf{u}_\mathrm{c}$ is the unit vector along the chord connecting $\mathcal{P}_1$ and $\mathcal{P}_2$. The figure shows that the locus of minimum departure velocities, $v_\mathrm{m} = \|\mathbf{v}_\mathrm{m}\|$, is tangent to the locus of solutions at the point where $K_1 = K_{1,\mathrm{min}}$. This was already anticipated by Prop. 3: the departure velocity for $\mathcal{S}_\mathrm{m}$ is the minimum among all possible transfers. Increasing the departure velocity yields two intersection points with the locus of solutions. When the velocity becomes equal to $\sqrt{2(1-\xi)/r}$ for $r = r_1$ the solutions are parabolic spirals, with

$$\mathbf{v}_\mathrm{p} = \sqrt{\frac{2(1-\xi)}{r_1}}\,(\cos\psi_1\, \mathbf{u}_1 + \sin\psi_1\, \mathbf{u}_2)$$

Here the vector $\mathbf{u}_2$ is defined by the inplane perpendicular to $\mathbf{u}_1$, in counter-clockwise direction, and ψ_1 is given in Eq. (28). The velocity v_Kep corresponds to the magnitude of the departure velocity for the minimum energy ellipse in the Keplerian case. It is observed that a spiral transfer allows to reduce the minimum velocity required for the transfer, $v_\mathrm{m} < v_\mathrm{Kep}$. The required Δv for leaving the departure orbit will be smaller than the one of the ballistic case. This is an important improvement with respect to the logarithmic spirals (Petropoulos *et al.*[13] and McInnes[14] show that logarithmic spirals typically require higher v_∞ at departure than the ballistic case). Increasing the magnitude of the departure velocity yields hyperbolic spiral transfers. This branch of solutions converges asymptotically to the chord connecting $\mathcal{P}_1$ and $\mathcal{P}_2$.

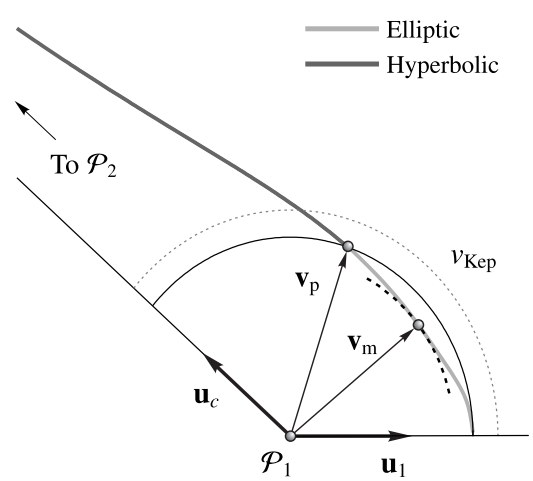

Figure 7: **Locus of velocity vectors on skewed axes and** $\xi = 1/2$

FIXING THE TIME OF FLIGHT

Generalized logarithmic spirals admit closed-form solutions for the time of flight, listed in Table 1 for convenience. They depend on the type of spiral. This section analyzes the spiral transfers from $\mathbf{r}_1$ to $\mathbf{r}_2$ given a constraint on the time of flight. The simplest solution is the transfer along a parabolic spiral ($K_1 = 0$), which corresponds to a logarithmic spiral. Combining Eqs. (13) and (28) the time of flight reduces to

$$t_2 = \pm \frac{2\sqrt{2(1-\xi)[\ln^2(r_2/r_1) + (\theta_2-\theta_1)^2]}}{3\ln(r_2/r_1)} \left(r_2^{3/2} - r_1^{3/2}\right) \tag{36}$$

This expression depends only on the boundary conditions and the control parameter.*

Figure 8 shows the influence of the constant of the energy in the time of flight from $\mathcal{P}_1$ to $\mathcal{P}_2$. As $K_1 \to 0^-$ the branch of fast solutions converges to the fast parabolic transfer. It defines the transition from elliptic to hyperbolic spirals. Note that $K_1 = 0$ behaves as a vertical asymptote: the parabolic solution along the slow branch requires an infinite time to reach $\mathcal{P}_2$. This is due to the fact that the slow parabolic transfer connects both points through infinity, as discussed from Fig. 4. Increasing K_1 from that point and along the slow branch yields the fictitious set of hyperbolic solutions that connect $\mathcal{P}_1$ and $\mathcal{P}_2$ through infinity. An entire family of solutions is found for every time of flight, simply changing the value of ξ.

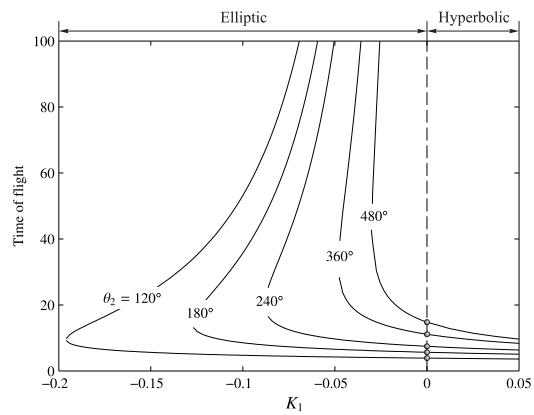

Figure 8: **Time of flight in terms of K_1**

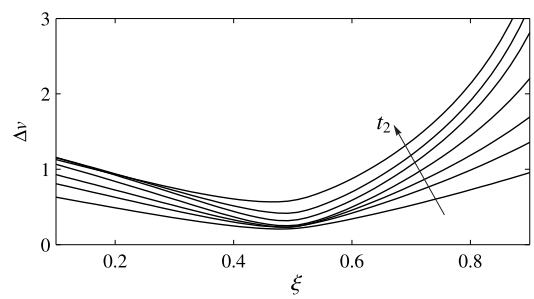

Figure 9: **Δv as a function of the control parameter for a given geometry**

The parameterization used to construct Fig. 8 shows that the time of flight does not have any minima. Given the time of flight and the geometry of the transfer the value of ξ can be changed to have different solutions for the same K_1. This statement holds for a given number of revolutions (defined as part of the geometry of the transfer) and for prograde orbits. There is an equivalent retrograde spiral transfer, $\psi_1 \in (\pi, 2\pi)$, with a different time of flight, unless the transfer is symmetric with respect to θ_1. Figure 8 suggests that different solutions to Lambert's problem can be obtained by changing the number of revolutions, i.e. the transfer angle. Similarly, Fig. 9 displays the Δv_{tot} for a family of solutions obtained by changing ξ, and having fixed the geometry and time of flight. It shows that, in general, there is a value of ξ that minimizes Eq. (33).

* In the limit case $r_2 = r_1$ and $\xi = 1/2$ this expression provides

$$\lim_{r_2 \to r_1} t_2 = \lim_{r_2 \to r_1} \frac{2}{3}(\theta_2 - \theta_1)\left[\frac{r_2^{3/2} - r_1^{3/2}}{\ln(r_2/r_1)}\right] = (\theta_2 - \theta_1)\, r_1^{3/2}$$

which is in fact the normalized time of flight corresponding to a circular Keplerian orbit of radius r_1.

The constraint on the time of flight leaves one degree of freedom (the value of ξ), apart from the number of revolutions and the selection of prograde/retrograde motion. The spiral Lambert's problem translates into solving for K_1 and ψ_1 in

$$r_2 = r(\theta_2; K_1, \xi, \psi_1, r_1, \theta_1) \tag{37}$$

$$t_2 = t(r(\theta_2); K_1, \xi, \psi_1, r_1, \theta_1) \tag{38}$$

The form of the functions $r(\theta)$ and $t(r)$ is summarized in Table 1. Recall that the transfer angle θ_2 accounts for the number of revolutions n, so that $\theta_2 = \tilde{\theta}_2 + 2n\pi$ with $\theta_2 \in [0, 2\pi]$.

The retrograde solutions can be found by solving a complementary problem where θ_2 is replaced by $\theta_{2,\text{ret}}$, defined as $\theta_{2,\text{ret}} = 2(n+1)\pi - \tilde{\theta}_2$. The solution to Eqs. (37) and (38) obtained for the complementary problem, $\psi_{1,\text{ret}}$, is modified so that it yields a retrograde orbit, i.e. $\psi_1 = 2\pi - \psi_{1,\text{ret}}$.

RESONANT TRANSFERS

The $\mathscr{T}$-symmetry of elliptic and Type II hyperbolic spirals allows finding resonant solutions to the two-point boundary-value problem. Assume that an elliptic spiral trajectory intersects the axis of symmetry in raising regime. Due to the $\mathscr{T}$-symmetry of the trajectory it will always intersect again the axis at that exact point in lowering regime after sufficient time. Hence, if the axis of symmetry is aligned with $\mathbf{r}_2$ and the spiral connects $\mathcal{P}_1$ and $\mathcal{P}_2$ in m revolutions, then it will always pass again through $\mathcal{P}_2$ after n revolutions. We refer to this as an $m:n$ resonant transfer. The departure flight-direction angle can be selected so that the integers m and n take certain values.

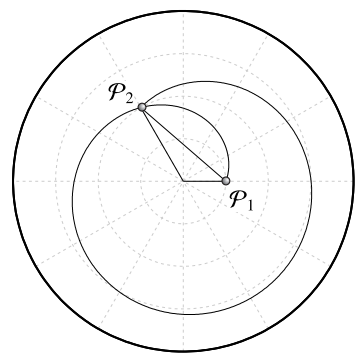

Figure 10: **Example of a** $0:1$ **resonant transfer**

When defining resonant transfers K_1 is fixed and cannot be decided at convenience: it depends on the geometry of the transfer. The simplest way to formulate the problem is to solve for K_1 and ψ_1 in the system:

$$r_2 = r(\tilde{\theta}_2 + 2m\pi; K_1, \psi_1, r_1, \theta_1)$$
$$r_2 = r(\tilde{\theta}_2 + 2n\pi; K_1, \psi_1, r_1, \theta_1)$$

The solution depends on the configuration of the $m:n$ resonance. Solutions only exist for elliptic spirals and hyperbolic spirals of Type II.

Figure 10 depicts an example of a resonant transfer. The solutions are indirect, by definition. If $m+n$ is even then the maximum is oriented in the direction of $\tilde{\theta}_2$, whereas if $m+n$ is odd then the maximum corresponds to $\tilde{\theta}_2 + \pi$. The magnitude of the maximum radius depends on $n-m$ and on the value of m, which indicates how soon the point $\mathcal{P}_2$ is reached for the first time.

Property 17: *(Arrival velocity for resonant transfers) Given a $m:n$ resonant transfer, the velocity at $\mathcal{P}_2$ is the same after m revolutions and after n revolutions.*

Property 18: *(Arrival flight-direction angle for resonant transfers) Let ψ_2 denote the flight-direction angle at $\mathcal{P}_2$ after m revolutions, and ψ_2' its value after n revolutions. Then $\psi_2 + \psi_2' = \pi$.*

Property 19: *(Thrust acceleration at $\mathcal{P}_2$ for resonant transfers) The magnitude of the thrust acceleration at $\mathcal{P}_2$ for resonant passes is the same, but one favors the velocity whereas the other opposes it.*

The search for resonant transfers is an additional technique for controlling the time of flight. Although the configuration of the transfer is given by discrete values of m and n, it might be useful for different mission scenarios. Figure 11 shows the time of flight for the two resonant passes, t_2 and t_2', for different indexes m and n. It is interesting to note that increasing the number of revolutions between the two passes reduces t_2, while the time of flight t_2' increases. For constant n increasing m yields slower transfers. Similarly, for constant m larger values of n increase the time of flight. When $m \to \infty$ the difference in the time of flight for the two resonant passes decreases, and the time of flight approaches a limit value. The existence of a finite limit relates to the fact that increasing the number of revolutions makes $K_{1,\min}$ smaller in magnitude until $\mathcal{S}_{\mathrm{m}}$ becomes parabolic in the theoretical limit (see Fig. 2).

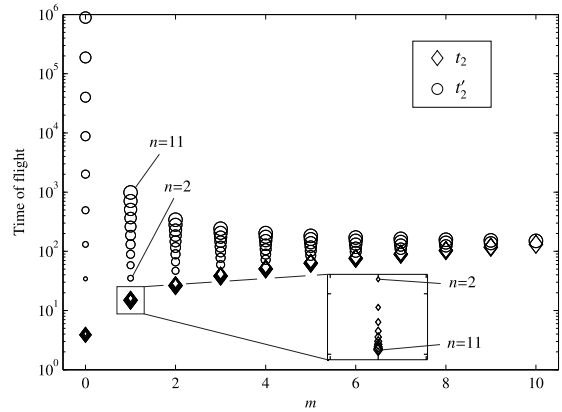

Figure 11: Time of flight for different $m : n$ resonant configurations. The size of the markers scales with the values of the index $n > m$. Diamonds represent the time to the first pass, and circles correspond to the second pass.

APPLICATIONS

Earth to Mars transfer opportunities

The problem of designing low-thrust transfers between two given bodies can be reduced to the spiral Lambert's problem, where the geometry of the transfer and the time of flight come from the configuration of the system at a given epoch. This technique is applied to finding launch opportunities to Mars. Given the Earth departure date and the Mars arrival date the boundary conditions $\mathbf{r}_1$ and $\mathbf{r}_2$, and the time of flight are fixed. This approach requires two additional impulsive maneuvers in order to leave the Earth and to rendezvous with Mars. The thrust is assumed tangential ($\xi = 1/2$).

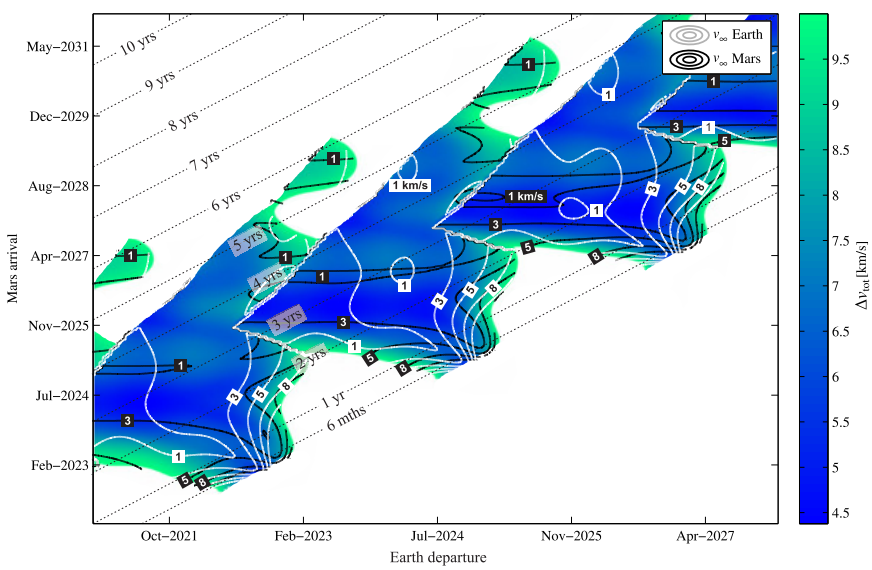

Figure 12: **Spiral transfer map from the Earth to Mars**

Figure 12 maps the required Δv for the corresponding Earth to Mars transfers. Woolley and

Nicholas[15] recently presented a more detailed map showing the delivered mass for different electric propulsion systems. They required about 4-10 hours of CPU time for solving 5,000 transfers. In the proposed simplified model using generalized logarithmic spirals it is possible to reduce the computational time down to about 1 or 2 minutes. Although less rigorous this method might be adequate for studying the preliminary space of solutions prior to applying more sophisticated tools. No numerical integration is required and the only iterative process is that applied to solving for K_1 and ψ_1. The solutions in the figure correspond to 0, 1, and 2 revolutions, and the one with the minimum Δv is plotted. By increasing the number of revolutions the minimum Δv regions can be expanded to stretch the launch windows. The optimal flight time is found to be between two and three years, which is similar to that reported by Woolley and Richards.[15]

Asteroid tour

Decomposing the design problem in a series of spiral Lambert's problems is interesting when a number of bodies are to be visited sequentially, for example for an asteroid tour. We present a hypothetical mission to visit four asteroids departing from the Earth. The duration of the mission is limited to 20 years in order to let the Lambert solver to choose the number of revolutions that minimizes the Δv_{tot}. Long times of flight allow multirevolution transfers and the solution will not be restricted to the zero-revolutions case.

Table 2 describes each spiral arc in terms of K_1, ψ_1 and the number of revolutions, n. The solution corresponds to quasi-circular spirals, as deduced from the values of the flight direction angle at departure. The spacecraft does not chase the asteroids but rather finds the adequate phasing to meet the asteroids in the vicinity of its quasi-circular trajectory. A purely tangential thrust ($\xi = 1/2$) is considered to limit the number of parameters.

Table 2: **Characteristics of each transfer leg**

Leg	K_1	ψ_1	n	TOF [days]	$a_{\text{p,max}}$ [μm/s^2]
#1	-3.2512×10^{-5}	89.99°	4	1713.0	2.5736
#2	$+8.8102 \times 10^{-6}$	90.01°	5	2093.7	3.7133
#3	$+4.3874 \times 10^{-4}$	89.93°	3	1559.0	27.286
#4	$+2.0625 \times 10^{-4}$	89.76°	2	1336.0	14.705

Figure 13 presents the time history of the thrust acceleration corresponding to the optimized solution. The small acceleration along the first and second legs is a consequence of how close to a circular orbit the solution is. This phenomenon reduces the discontinuity in the transition between the two first spiral arcs, requiring a correcting maneuver of only 18.6 m/s. The plane changes for the last two transfers require higher Δv's. About 1,000 tours can be evaluated per minute.

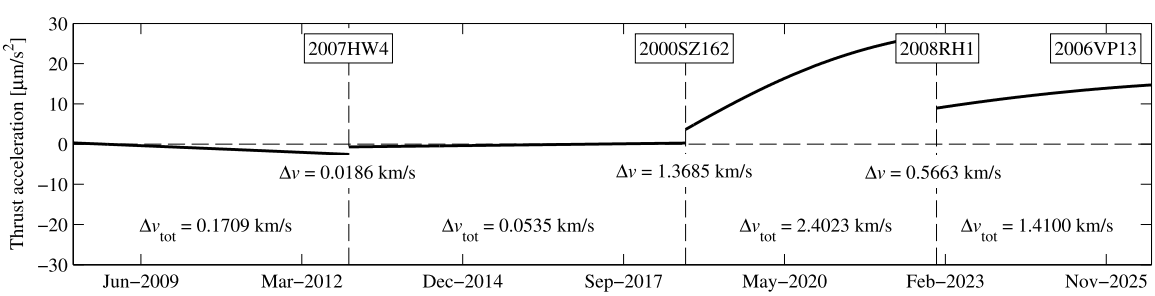

Figure 13: **Timeline for the asteroid tour mission**

CONCLUSIONS

The connections with the Keplerian case found in the definition of the family of generalized logarithmic spirals simplify the study of the spiral Lambert's problem. The existence of two integrals of motion provides a clear structure of the solution and yields dynamical properties of theoretical and practical interest. Classical geometric and dynamic properties of the Keplerian Lambert's problem have an equivalent expression in spiral form. All the numerical computations reduce to solving a system of two equations with two unknowns. No other iterative processes are required. The numerical procedure is simplified thanks to having located special cases for which the transfer can be solved analytically or there is a specific numerical procedure to compute them. When the time of flight is fixed there is still a degree of freedom in the solution. The main advantage of the method for computing low-thrust transfers presented in this paper is its speed and intuitive use. This technique provides a simple tool for exploring wide spaces of solutions that would be intractable otherwise. Global searches and optimization scenarios are some examples of problems where a cost function that is expensive to evaluate will restrict the search process.

ACKNOWLEDGEMENT

This work has been carried out at the Jet Propulsion Laboratory within the framework of the JVSRP program. It is part of the research project entitled "Dynamical Analysis, Advanced Orbit Propagation and Simulation of Complex Space Systems" (ESP2013-41634-P) supported by the Spanish Ministry of Economy and Competitiveness. Authors thank the Spanish Government for its support and J. Roa especially thanks "La Caixa" for his doctoral fellowship. They are indebted to J. Senent for motivating this work, and thank A. Petropoulos, N. Arora and J. Sims for their advice.

REFERENCES

[1] R. H. Battin, "Lambert's problem revisited," *AIAA J*, Vol. 15, No. 5, 1977, pp. 707–713.

[2] R. H. Battin and R. M. Vaughan, "An elegant Lambert algorithm," *J Guid Control Dynam*, Vol. 7, No. 6, 1984, pp. 662–670, 10.2514/3.19910.

[3] R. H. Battin, *An introduction to the mathematics and methods of Astrodynamics*. AIAA, 1999.

[4] E. Lancaster, R. Devaney, and R. Blanchard, "A note on Lambert's theorem.," *J Spacecraft Rockets*, Vol. 3, No. 9, 1966, pp. 1436–1438, 10.2514/3.28673.

[5] R. Gooding, "A procedure for the solution of Lambert's orbital boundary-value problem," *Celest Mech Dyn Astr*, Vol. 48, No. 2, 1990, pp. 145–165, 10.1007/BF00049511.

[6] D. Izzo, "Revisiting Lambert's problem," *Celest Mech Dyn Astr*, Vol. 121, No. 1, 2014, pp. 1–15.

[7] D. Izzo, "Lambert's problem for exponential sinusoids," *J Guid Control Dynam*, Vol. 29, No. 5, 2006, pp. 1242–1245, 10.2514/1.21796.

[8] A. E. Petropoulos and J. M. Longuski, "Shape-based algorithm for the automated design of low-thrust, gravity assist trajectories," *J Spacecraft Rockets*, Vol. 41, No. 5, 2004, pp. 787–796, 10.2514/1.13095.

[9] J. Roa and J. Peláez, "Generalized logarithmic spirals for low-thrust trajectory design," *AAS/AIAA Astrodynamics Specialist Conference*, No. 15-729, 2015.

[10] J. Roa, J. Peláez, and J. Senent, "Generalized logarithmic spirals for low-thrust trajectory design," *J Guid Control Dynam*, 2015.

[11] J. Roa and J. Peláez, "Introducing a degree of freedom in the family of generalized logarithmic spirals," *26th Spaceflight Mechanics Meeting*, No. 16-317, 2016.

[12] J. Roa and J. Peláez, "Three-dimensional generalized logarithmic spirals," *26th Spaceflight Mechanics Meeting*, No. 16-323, 2016.

[13] A. E. Petropoulos, J. M. Longuski, and N. X. Vinh, "Shape-based analytic representations of low-thrust trajectories for gravity-assist applications," *AAS/AIAA Astrodynamics Specialist Conference*, 1999, pp. 563–581.

[14] C. R. McInnes, *Solar sailing: technology, dynamics and mission applications*. Springer Science & Business Media, 2004.

[15] R. Woolley and A. Nicholas, "SEP mission design space for Mars orbiters," *Adv Astronaut Sci*, 2015, pp. AAS15–632.